JACS
JOURNAL OF THE AMERICAN CHEMICAL SOCIETY
Article
pubs.acs.org/JACS

Intramolecular Energy and Electron Transfer within a Diazaperopyrenium-Based Cyclophane

Xirui Gong,[†,#] Ryan M. Young,[†,‡,#] Karel J. Hartlieb,[†] Claire Miller,[†,‡] Yilei Wu,[†,‡] Hai Xiao,[§] Peng Li,[†] Nema Hafezi,[†] Jiawang Zhou,[†,‡] Lin Ma,[†,‡] Tao Cheng,[§] William A. Goddard, III,[§] Omar K. Farha,[†,∥] Joseph T. Hupp,[†] Michael R. Wasielewski,*[,†,‡] and J. Fraser Stoddart*[,†]

[†]Department of Chemistry and [‡]Argonne-Northwestern Solar Energy Research (ANSER) Center, Northwestern University, 2145 Sheridan Road, Evanston, Illinois 60208, United Sates

[∥]Department of Chemistry, Faculty of Science, King Abdulaziz University, Jeddah 22254, Saudi Arabia

[§]Materials and Process Simulation Center, California Institute of Technology, Pasadena, California 91125, United States

Supporting Information

ABSTRACT: Molecules capable of performing highly efficient energy transfer and ultrafast photoinduced electron transfer in well-defined multichromophoric structures are indispensable to the development of artificial photofunctional systems. Herein, we report on the synthesis, characterization, and photophysical properties of a rationally designed multichromophoric tetracationic cyclophane, **DAPPBox**$^{4+}$, containing a diazaperopyrenium (DAPP^{2+}) unit and an extended viologen (ExBIPY^{2+}) unit, which are linked together by two *p*-xylylene bridges. Both ^{1}H NMR spectroscopy and single-crystal X-ray diffraction analysis confirm the formation of an asymmetric, rigid, box-like cyclophane, **DAPPBox**$^{4+}$. The solid-state superstructure of this cyclophane reveals a herringbone-type packing motif, leading to two types of $\pi\cdots\pi$ interactions: (i) between the ExBIPY^{2+} unit and the DAPP^{2+} unit ($\pi\cdots\pi$ distance of 3.7 Å) in the adjacent parallel cyclophane, as well as (ii) between the ExBIPY^{2+} unit ($\pi\cdots\pi$ distance of 3.2 Å) and phenylene ring in the closest orthogonal cyclophane. Moreover, the solution-phase photophysical properties of this cyclophane have been investigated by both steady-state and time-resolved absorption and emission spectroscopies. Upon photoexcitation of **DAPPBox**$^{4+}$ at 330 nm, rapid and quantitative intramolecular energy transfer occurs from the ^{1}*ExBIPY^{2+} unit to the DAPP^{2+} unit in 0.5 ps to yield ^{1}*DAPP^{2+}. The same excitation wavelength simultaneously populates a higher excited state of ^{1}*DAPP^{2+} which then undergoes ultrafast intramolecular electron transfer from ^{1}*DAPP^{2+} to ExBIPY^{2+} to yield the DAPP$^{3+\bullet}$−ExBIPY$^{+\bullet}$ radical ion pair in τ = 1.5 ps. Selective excitation of DAPP^{2+} at 505 nm populates a lower excited state where electron transfer is kinetically unfavorable.

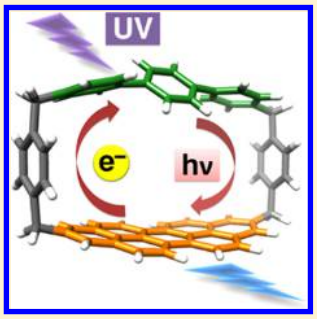

INTRODUCTION

The construction of well-organized multichromophoric architectures, capable of performing efficient energy transfer (EnT) and electron transfer[1] (ET), is an indispensable part of the development of photofunctional systems. The key to the design of such synthetic systems is controlling the electronic interactions between donors (D) and acceptors (A) to optimize efficient EnT and /or ET. Encouraging progress has been made on the construction of photofunctional systems, extending from discrete (1D) to extended (2D and 3D) structures, such as π-stacked molecules,[2] covalently linked porphyrin arrays,[3] dendrimers,[4] chromophoric polymers,[5] self-assembled structures,[6] and hybrid organic−inorganic structures.[7] Recently, the photophysical properties (either EnT or ET) of a newly synthesized tetracationic cyclophane, **ExBox**$^{4+}$, and its supramolecular complexes have been investigated.[8] **ExBox**$^{4+}$ is related to cyclobis(paraquat-*p*-phenylene) wherein the 4,4′-bipyridinium units have been replaced with an extended *p*-phenylene-bridged bipyridinium unit, ExBIPY^{2+}. Multielectron accumulation[7e] and photoinduced charge shift reactions of **ExBox**$^{4+}$ have been demonstrated by intramolecular[9] through-bond electron transfer from the *p*-xylylene bridges to the extended bipyridinium units (ExBIPY^{2+}) within **ExBox**$^{4+}$ itself as well as by intermolecular[6c] photoinduced charge shift within perylene⊂**ExBox**$^{4+}$ complexes. On the other hand, EnT processes have been observed[6e,f] in supramolecular systems, by binding **ExBox**$^{4+}$ to other chromophores, like perylene-3,4:9,10-bis(dicarboximide)s (PDIs) (Figure 1a). Although one of the ExBIPY^{2+} units in **ExBox**$^{4+}$ can undergo intramolecular photoinduced charge separation if excited with UV light, optimum utilization of the solar spectrum for artificial photosynthesis requires systems that absorb at wavelengths >400 nm. Given this requirement, we have designed an asymmetric cyclophane which incorporates one ExBIPY^{2+} (Figure 1b) electron acceptor unit. For a second chromophore to work alongside an ExBIPY^{2+} unit within the geometry of a cyclophane molecule, that chromophore must satisfy several criteria. First of all, the chromophore must be able to form a donor−acceptor pair with an ExBIPY^{2+} unit. Second, it should have a similar

Received: December 31, 2016
Published: February 22, 2017

DOI: 10.1021/jacs.6b13223
J. Am. Chem. Soc. 2017, 139, 4107−4116

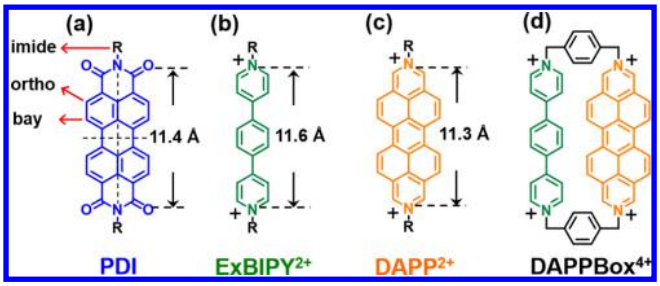

Figure 1. Structural formulas of (a) **PDI**, (b) **ExBIPY**$^{2+}$, (c) **DAPP**$^{2+}$, and (d) **DAPPBox**$^{4+}$.

length as an ExBIPY^{2+} unit to ensure that the cyclophane retains its rectangular shape, which (i) promotes good electronic coupling between the donor and acceptor in the face-to-face geometry as well as (ii) provides an opportunity to bind guests, which may be used to modulate the coupling between the donor and the acceptor, thereby allowing control over charge separation and recombination rates.[6c]

A class of molecules that match the above criteria are the diazaperopyrenium dications,[10] shown in Figure 1c. Although these dications are structurally related and share optical properties similar to those of the PDIs, they possess enhanced solubility as a result of their dicationic nature. Additionally, DAPP^{2+} dications can be dissolved selectively either in organic solvents (soft counterions, e.g., PF_6^-, BF_4^-) or in aqueous environments (hard counterions, e.g., $CF_3CO_2^-$, Cl^-). Since energy transfer between ExBIPY^{2+} and PDI has been described[6e,f] in self-assembled systems, we expect that, by incorporating a DAPP^{2+} dicationic unit into a constitutionally asymmetric cyclophane along with an ExBIPY^{2+} unit, the unique arrangement of multichromophoric units could demonstrate special photophysical properties, while avoiding solubility issues commonly associated with PDIs.[11] The known properties[10e] of the DAPP^{2+} dication suggest these dicationic units are suitable substitutes for PDIs for incorporation into multichromophoric cyclophanes.

Here, we report a rational design and preparation of a cyclophane, **DAPPBox**$^{4+}$ (Figure 1d), containing one DAPP^{2+} unit and one ExBIPY^{2+} unit, which are bridged together by two *p*-xylylene linkers. This constitutionally asymmetric tetracationic cyclophane is readily soluble in both organic solvents, e.g., MeCN, $MeNO_2$, and DMF, as a PF_6^- salt, and in water as a Cl^- or TFA^- salt. In this investigation, we have combined steady-state measurements, visible and near-infrared (NIR) transient absorption spectroscopy, and electronic structure calculations in order to investigate the photophysical processes within **DAPPBox**$^{4+}$. Our results show that photoexcitation of the ExBIPY^{2+} electron acceptor within DAPPBox^{4+} results in ultrafast energy transfer to the lowest excited state of the DAPP^{2+} electron donor, followed by competitive fluorescence and intersystem crossing. Owing to the overlapping absorption of the subunits at 330 nm, excitation at this wavelength also leads to a small population of highly excited ^{1}*DAPP^{2+} which decays by electron transfer to DAPP$^{3+\bullet}$–ExBIPY$^{+\bullet}$ in τ = 1.5 ps. Electron transfer from the lowest excited state of ^{1}*DAPP^{2+} around 2.46 eV is kinetically unfavorable in the cyclophane, leading to the same decay previously observed in DAPP^{2+}. This rationally designed **DAPPBox**$^{4+}$ can perform both energy- and electron-transfer processes. The detailed study of the photophysical properties of the cyclophane constitutes an important fundamental step toward the understanding of competitive photophysical processes in the context of controlled molecular geometries.

RESULTS AND DISCUSSION

Synthesis of the DAPPBox·4PF$_6$. The synthesis of **DAPPBox**$^{4+}$ is outlined in Scheme 1. Briefly, S_N2 reactions between an excess of 3,4,9,10-tetrakis(chloromethyl)perylene (**1**) and 4-(aminomethyl)benzenemethanol (**2**) in Me_2SO at room temperature for 5 h, lead to the formation of **3**. Subsequently, **3** is oxidized by 2,3-dichloro-5,6-dicyano-1,4-benzoquinone (DDQ) in DMF at room temperature for 8 h to afford, after counterion exchange, **4**·2PF$_6$. Bromination of **4**·2PF$_6$ with PBr_3 in MeCN at room temperature overnight, followed by counterion exchange with NH_4PF_6, results in the fomation of the dibromide **BrDAPP**·2PF$_6$. Finally, pyrene-templated[8b] cyclization between **BrDAPP**·2PF$_6$ and 4,4′-(1,4-phenylene)bispyridine (ExBIPY) in MeCN at room temperature for 7 days, followed by precipitation of the crude product with tetrabutylammonium chloride (TBACl), gives pyrene⊂**DAPPBox**·4Cl. This complex can then be dissolved in H_2O and the aqueous solution subjected to continuous extraction with $CHCl_3$ for 3 days in order to remove the pyrene guest molecule from the cyclophane. The desired product **DAPPBox**·4PF$_6$ was isolated by reverse-phase column chromatography, followed by counterion

Scheme 1. Synthesis of DAPPBox·4PF$_6$

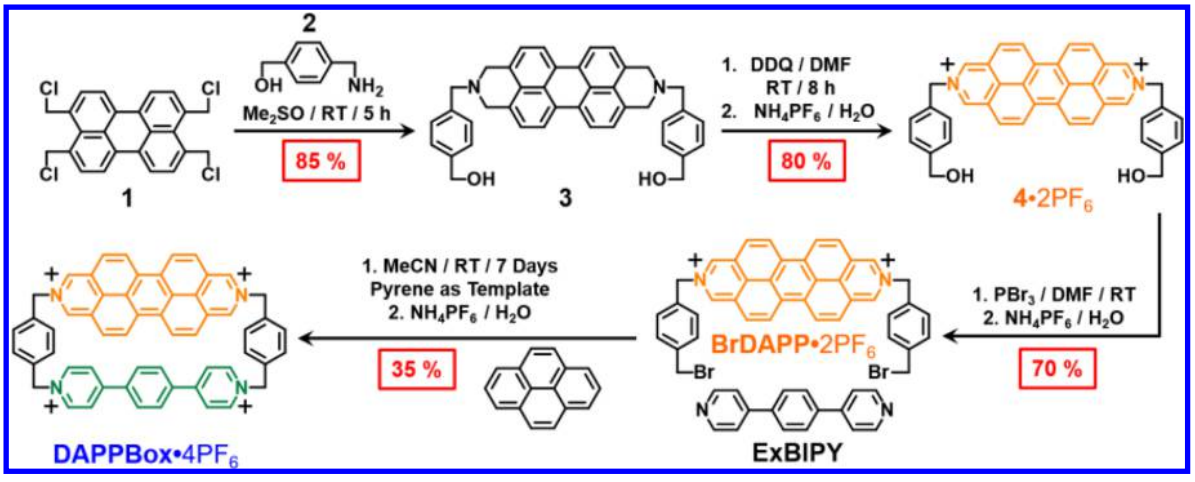

DOI: 10.1021/jacs.6b13223
J. Am. Chem. Soc. 2017, 139, 4107–4116

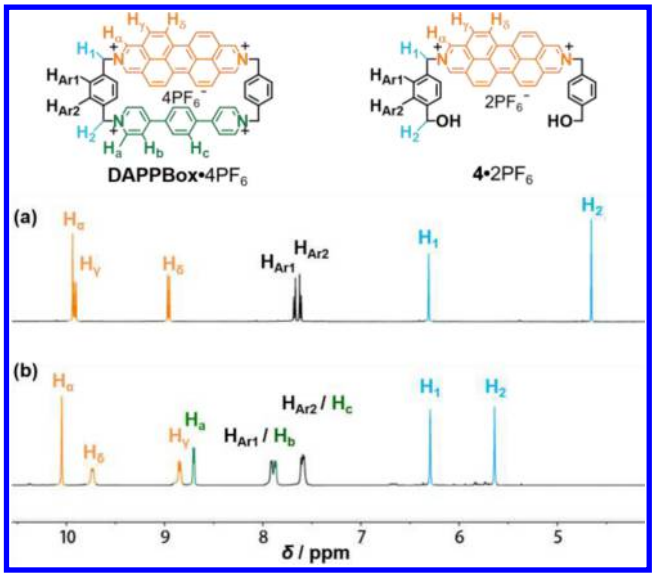

Figure 2. ^{1}H NMR spectra of (a) **4**·2PF$_6$ and (b) **DAPPBox**·4PF$_6$ (500 MHz, CD_3CN, 298 K).

exchange (NH_4PF_6/H_2O) in 35% yield. The formation of **DAPPBox**·4PF$_6$ was confirmed by recording the ^{1}H NMR spectrum (Figure 2) in MeCN at room temperature. The peaks in the spectrum were assigned on the basis of analyses of two-dimensional ^{1}H–^{1}H COSY NMR (Figure S1a) and 2D NOESY NMR (Figure S1b) spectra. As a result of its asymmetric constitution, two sets of peaks can be assigned to the methylene protons (H_1/H_2, δ = 6.27/5.63 ppm) as well as another two sets of peaks to the phenylene protons (H_{Ar1}/H_{Ar2}, δ = 7.87/7.59 ppm) of the *p*-xylylene linkers. High-resolution mass spectrometry (HRMS) revealed the presence of the $[M - PF_6]^+$, $[M - 2PF_6]^{2+}$, and $[M - 3PF_6]^{3+}$ species which were detected at m/z = 1203.2074, 529.1266, and 304.4293, respectively.

Further evidence for cyclophane formation comes from single-crystal X-ray diffraction (XRD), Figure 3. Single crystals were grown by vapor diffusion of *i*-Pr_2O into an MeCN solution of **DAPPBox**·4TFA during 1 week. The solid-state structure (Figure 3a) reveals an asymmetric, box-like cyclophane, with average dimensions of 14.1 Å × 7.1 Å (Figure 3b). The two torsional angles between the pyridinium and the *p*-phenylene rings are ∼17° and ∼20° (Figure 3c), respectively; i.e., they are smaller than the average torsional angle (∼30°)[8a] in **ExBox**$^{4+}$. This flatter conformation for the ExBIPY^{2+} unit in **DAPPBox**$^{4+}$ is probably a consequence of intermolecular $\pi\cdots\pi$ interactions[12] between the ExBIPY^{2+} unit and adjacent cyclophanes. The *p*-xylylene ring in the closest adjacent cyclophane ($\pi\cdots\pi$ distance of 3.2 Å) is associated with a torsional angle of ∼17° in the ExBIPY^{2+} unit, while the larger torsional angle (∼20°) is adjacent to the relative weaker intermolecular aromatic recognition ($\pi\cdots\pi$ distance of 3.7 Å) between the ExBIPY^{2+} unit and the DAPP^{2+} unit in another adjacent cyclophane. The perspective view of the solid-state superstructure (Figure 3d) of **DAPPBox**$^{4+}$ reveals only partial $\pi\cdots\pi$ overlap between the ExBIPY^{2+} unit and a DAPP^{2+} unit in a neighboring cyclophane, most likely arising from the balance between Coulombic repulsions and the maximization of π-overlap.[10h] The overall

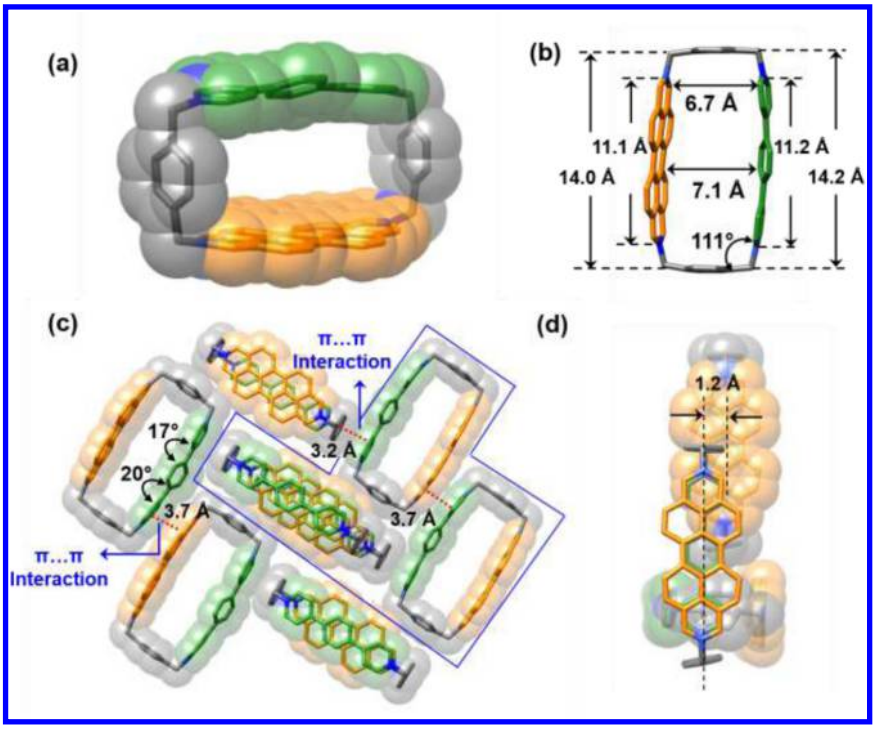

Figure 3. Solid-state (super)structure of the **DAPPBox**$^{4+}$ obtained from X-ray crystallography on single crystals of **DAPPBox**·4TFA. (a) Perspective view of the **DAPPBox**$^{4+}$ as a stick representation with the corresponding semitransparent space-filling representations superimposed upon it. (b) Plan view of stick representation DAPPBox^{4+} ring showing distances and torsional angles associated with the ring's geometry. (c) Solid-state superstructure of **DAPPBox**$^{4+}$ revealing a herringbone type of packing and two types of $\pi\cdots\pi$ interactions[12] as labeled above, resulting in flatter features for the ExBIPY^{2+} unit (smaller torsional angle between adjacent pyridinium rings, ∼17° and ∼20°, respectively) in **DAPPBox**$^{4+}$, compared[8a] (∼30°) with its **ExBox**$^{4+}$ analogue. (d) Perspective view of the superstructure of **DAPPBox**$^{4+}$ demonstrating the partial overlap between the ExBIPY^{2+} and DAPP^{2+} units in adjacent cyclophanes, probably resulting from the balance between Coulombic repulsions and the maximization of π-overlap.

DOI: 10.1021/jacs.6b13223
J. Am. Chem. Soc. 2017, 139, 4107–4116

superstructure of $DAPPBox^{4+}$ reveals a herringbone type of packing.

The templating role played by pyrene during the synthesis of the cyclophane is supported by the solid-state superstructure (Figure S5) of the complex, pyrene⊂**DAPPBox**·$4PF_6$. Single crystals, suitable for X-ray crystallography, were obtained by slow vapor diffusion of iPr_2O into a $MeNO_2$ solution of the complex. The superstructure reveals that pyrene sits inside the box at distances of 3.4 Å from the $DAPP^{2+}$ plane and 3.6 Å from the center of the $ExBIPY^{2+}$ unit. For full details, see the Supporting Information. In addition, the characteristic ^1H NMR signals of the macrocycle shift upon addition of pyrene (Figure S2), proving that complexation occurs between pyrene and **DAPPBox**$^{4+}$ in solution. A UV/vis absorption-based Job plot (Figure S3b) confirms the 1:1 stoichiometry between **DAPPBox**$^{4+}$ and pyrene in MeCN, an observation which is in agreement with the solid-state superstructure. Furthermore, the fluorescence titration (Figure S3c) carried out upon the addition of pyrene into an MeCN solution of the **DAPPBox**$^{4+}$ (excitation at 440 nm) shows a decrease of $DAPP^{2+}$ fluorescence (515 nm), accompanied by a slight blue shift of the emission maxima, caused by either electronic perturbation or structural distortion upon host−guest formation. Based on fluorescence titration data, the binding affinity K_a of complexation was calculated[11b] (Figure S3d) to be $(3.73 \pm 0.35) \times 10^5\ M^{-1}$.

Reference Compound Absorption and Emission. Two groups of reference compounds with methyl groups (Figure 4a) and benzyl groups (Figure 4b) attached to the nitrogen atoms in the 2 and 9 positions[10h] were investigated to understand the basic photophysical processes involved in each chromophore. Based on the results obtained from these reference compounds, we observed that the benzyl groups enable an ET deactivation pathway, a feature which was not found to be present in the corresponding methylated reference compound.[9] Thus, the photophysics of the methylated reference compounds (**Me-ExBIPY**$^{2+}$ and **Me-DAPP**$^{2+}$) were compared to that of **DAPPBox**$^{4+}$, when 330 nm photons were used to excite $ExBIPY^{2+}$, while the photophysics of the benzylated reference compounds (**Bn-ExBIPY**$^{2+}$ and **Bn-DAPP**$^{2+}$) were compared to that of $DAPPBox^{4+}$, when $DAPP^{2+}$ was selectively excited at 505 and 414 nm. Our data show that, in MeCN at room temperature, $Bn\text{-}ExBIPY^{2+}$ exhibits weak UV fluorescence (λ_{max} = 378 nm, Φ_{fl} = 3.8%), presumably as a result of deactivation by photoinduced electron transfer from the benzyl rings to $ExBIPY^{2+}$,[9] while strong UV emission is observed (λ_{max} = 364 nm, τ = 1.56 ns, Φ_{fl} = 69%, Figure S10) in the case of **Me-ExBIPY**$^{2+}$, where the electron-transfer pathway is not present. Conversely, neither methyl nor benzyl substituents significantly affect the $DAPP^{2+}$ behavior in either **Me-DAPP**$^{2+}$ (λ_{max} = 505 nm, τ = 17.6 ns, Φ_{fl} = 66%, Figure S11) or **Bn-DAPP**$^{2+}$ (λ_{max} = 509 nm, τ = 19.8 ns, Φ_{fl} = 60%, Figure S12), both of which show strong green fluorescence, so electron transfer from these species is unlikely (*vide infra*).

Some of the relevant photophysical data for all the compounds investigated are summarized in Table 1, where the emission maxima refer to the spectra corrected for instrument detection response. The UV/vis absorption spectrum of the model compounds **Me-ExBIPY**$^{2+}$ and **Me-DAPP**$^{2+}$, and the cyclophane **DAPPBox**$^{4+}$, recorded in MeCN are shown in Figure 5. The absorption bands for **Me-ExBIPY**$^{2+}$ occur at wavelengths shorter than 350 nm, with the maximum centered on 323 nm. The absorption spectrum for **Me-DAPP**$^{2+}$ is characterized by an intense band in the visible region, which is assigned to the $S_2 \leftarrow S_0$ electronic transition (λ_{max} = 438 nm), and in the UV region (<325 nm), assigned to the $S_n \leftarrow S_0$ electronic transition (λ_{max} = 296 nm). The exact ordering of the upper state accessed in this transition is left unassigned. The absorption of the $DAPPBox^{4+}$ exhibits minor differences when compared with the sum of the spectra of the corresponding model compounds, with only a slight red-shift of the absorption

Table 1. Photophysical Properties of the Reference Compounds and DAPPBox^{4+}

compound	λ_{abs} (nm)[a]/ ε_{max} (10^4 M^{-1} cm^{-1})	λ_{ems} (nm)[a]	τ (ns)[b]/ λ_{exc} (nm)[a]	Φ_{ems}[c]
Me-ExBIPY^{2+}	323/3.15	364	1.56/330	0.69
Me-DAPP^{2+}	438/5.66	505	17.6/375	0.66
Bn-ExBIPY^{2+}	321/2.31	378	0.062/330	0.04
Bn-DAPP^{2+}	443/5.74	509	19.8/375	0.60
DAPPBox^{4+}	442/4.98	520	19.5/374	0.39

[a] λ_{abs}, λ_{ems}, and λ_{exc} are the maximum absorption, emission, and excitation wavelengths. [b] τ is the fluorescence lifetime. [c] Φ_{ems} is the fluorescence quantum yield.

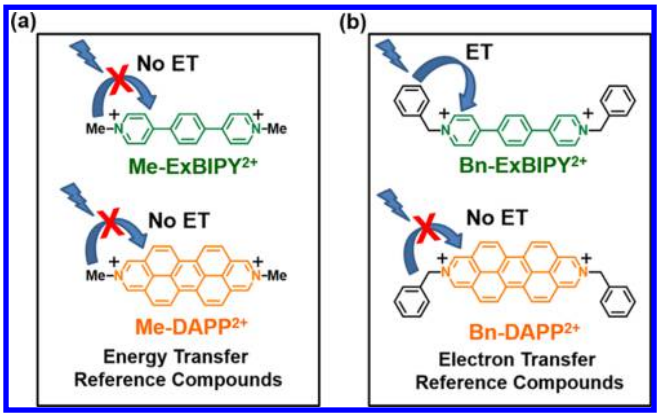

Figure 4. (a) Structural formulas of **Me-ExBIPY**$^{2+}$ and **Me-DAPP**$^{2+}$, which were used as reference compounds for the EnT process within **DAPPBox**$^{4+}$. (b) Structural formulas of **Bn-ExBIPY**$^{2+}$ and **Bn-DAPP**$^{2+}$, which were used as reference compounds for the ET process within **DAPPBox**$^{4+}$.

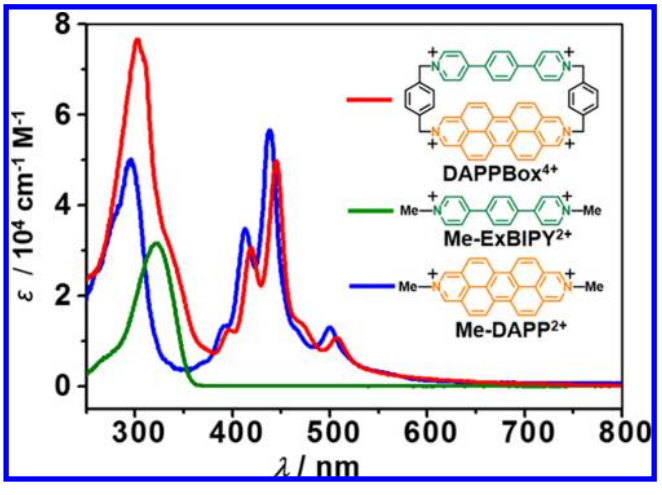

Figure 5. Absorption spectra of **DAPPBox**$^{4+}$, **Me-ExBIPY**$^{2+}$, and **Me-DAPP**$^{2+}$ in MeCN at room temperature.

DOI: 10.1021/jacs.6b13223
J. Am. Chem. Soc. 2017, 139, 4107−4116

maximum (λ_{max} = 446 nm). Importantly, from the reference compounds we see that at 330 nm, approximately 86% of the net extinction coefficient of **DAPPBox**$^{4+}$ can be assigned to the ExBIPY^{2+} subunit, while the remaining 14% can be attributed to the DAPP^{2+} absorption. Thus, we expect the excited states of each unit to participate in the dynamics following excitation.

Excited-State Dynamics. The excited-state dynamics of **DAPPBox**$^{4+}$ and its subunits were probed by femtosecond and nanosecond transient absorption (fsTA/nsTA) spectroscopies. The fsTA spectra (Figures S15a and 18a) of both **Me-DAPP**$^{2+}$ and **Bn-DAPP**$^{2+}$, following excitation at 330 nm, show similar spectral features: the ground-state bleach appears at 505 nm overlapping with the singlet excited-state absorption band, which spans from 450 to 900 nm and at 1440 nm. **Me-DAPP**$^{2+}$ and **Bn-DAPP**$^{2+}$ both show rapid internal conversion to a hot $^*S_1$ state, followed by structural relaxation prior to decay of their singlet states (Figures S15a and S18a). The ~20 ns singlet-state lifetimes for both DAPP^{2+} derivatives are longer than the maximum pump−probe delay time (~8 ns) of the fsTA experiment. The corresponding nsTA spectra (Figures S15b and S18b) show that the ^{1}***Me-DAPP**$^{2+}$ and ^{1}***Bn-DAPP**$^{2+}$ singlet states decay to their respective triplet states with time constants similar to those observed by time-resolved fluorescence; the triplet states then decay back to the ground state in approximately 250 and 220 ns, respectively, in air-equilibrated solutions at room temperature, presumably by collisional triplet−triplet annihilation and/or oxygen quenching. The reasonably intense triplet signals are commensurate with the moderate fluorescence quantum yields for **Me-DAPP**$^{2+}$ and **Bn-DAPP**$^{2+}$, as well as with the previous observation[10c] of the triplet state of DAPP^{2+}.

The transient absorption spectrum of **Bn-ExBIPY**$^{2+}$ excited at 330 nm is shown in Figure S21.[7e] The spectrum is initially dominated by an intense peak at 495 nm and a weaker feature around 1440 nm, which are assigned to the $S_n \leftarrow S_1$ absorption. These features decay in τ = 62 ± 1 ps as new bands peaking at 506 and 1110 nm appear. The spectra at this point strongly resemble ExBIPY$^{+\bullet}$,[7e] which confirms that fluorescence quenching of the ^{1}***Bn-ExBIPY**$^{2+}$ occurs by forward electron transfer. Back electron transfer occurs in 1200 ps, with some fraction recombining to the triplet state ($T_n \leftarrow T_1$, 480 nm).

The fsTA spectra of **DAPPBox**$^{4+}$ following 330 nm excitation appear (Figure 6a) very similar in both **Me-DAPP**$^{2+}$ and **Bn-DAPP**$^{2+}$. The absorption band present at ~1545 nm (Figure 6a) in the fsTA spectra of **DAPPBox**$^{4+}$ persists for the entire singlet-state lifetime (~20 ns), which is most likely the $S_n \leftarrow S_1$ excited-state absorption of the DAPP^{2+} unit. The most noticeable difference is a pronounced, rapid decay of the absorption at 495 nm, with the appearance of a new absorption at 1150 nm. The 495 nm signal decays on a slower time scale, which is similar to that observed for the singlet decay of excited DAPP^{2+} chromophores. The 1150 nm band appears within the ~200 fs instrument response and exhibits multiple decay components. As in the **Me-DAPP**$^{2+}$ and **Bn-DAPP**$^{2+}$ reference compounds, ^{1}*DAPP^{2+} decays to the triplet with an approximately 20 ns lifetime, and the triplet decays back to the ground state within 200 ns. Notably, the kinetics are more complicated in **DAPPBox**$^{4+}$ because of the overlapping ground-state absorptions at the excitation wavelength (Figure 6).

To remove complications from the parallel excitations at 330 nm, we acquired the fsTA spectra of **DAPPBox**$^{4+}$ following excitation at 505 nm (Figure 6b), and separately at 414 nm (Figure S19). The spectra resemble those of both **Me-DAPP**$^{2+}$

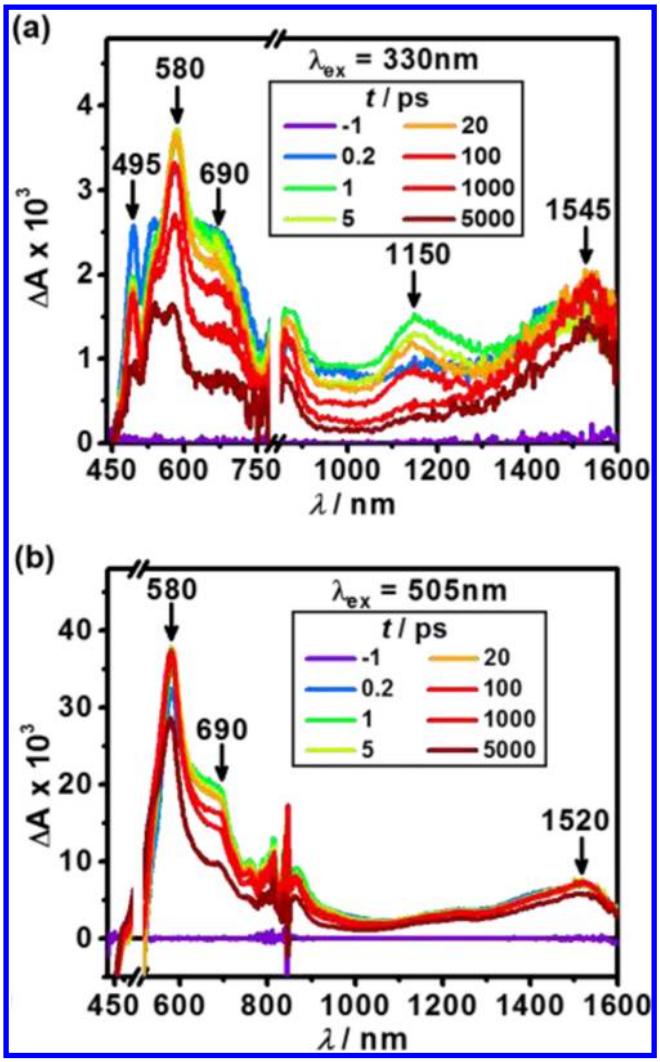

Figure 6. Visible and NIR spectra: (a) fsTA, 330 nm excitation, and (b) fsTA, 505 nm excitation spectra of **DAPPBox**$^{4+}$ in MeCN at room temperature. In (a), the spectra beyond 850 nm are scaled by a factor of 2 for clarity.

and **Bn-DAPP**$^{2+}$. Excitation at 414 nm again leads to rapid internal conversion to a hot $^*S_1$ state. There is a slower structural relaxation due to the rigid conformation of the box, followed by similar singlet-state and triplet-state lifetimes, 18 and 250 ns, respectively. Importantly, both the rapid decay of the peak at 495 nm and the new peak at 1150 nm that were observed when exciting at 330 nm are absent. This observation implies that exciting at lower photon energy shuts off some decay pathway(s), despite still exciting above the lowest energy excited state of DAPP^{2+}.

Efficient Energy Transfer within DAPPBox^{4+}**.** We expected an available EnT decay pathway (Figure 7a) from comparison of the emission spectra (λ_{exc} = 554 nm) in Figure 7b of **DAPPBox**$^{4+}$ with that of methylated reference compounds. Indeed, the emission spectrum of **DAPPBox**$^{4+}$ is devoid of UV fluorescence and is dominated by green emission (τ = 19.5 ns, Φ_{fl} = 39%, Figures S9) at 517 nm, even when the excitation occurs at ExBIPY^{2+} absorption wavelengths (λ_{exc} = 339 nm). The quenching of ExBIPY^{2+} fluorescence at 380 nm, accompanied by the enhancement of the DAPP^{2+} unit emission at 510 nm in the steady-state emission spectrum of **DAPPBox**$^{4+}$, suggests efficient singlet EnT from the ExBIPY^{2+} to the

DOI: 10.1021/jacs.6b13223
J. Am. Chem. Soc. 2017, 139, 4107−4116

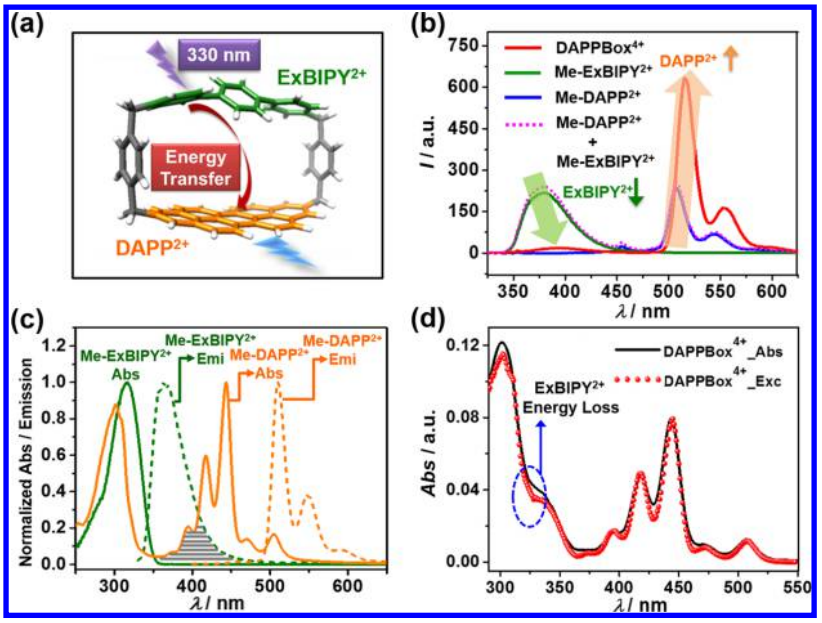

Figure 7. (a) Energy-transfer process within **DAPPBox**$^{4+}$. (b) Emission spectra of **DAPPBox**$^{4+}$, **Me-ExBIPY**$^{2+}$, **Me-DAPP**$^{2+}$, and a physical mixture of **Me-ExBIPY**$^{2+}$ and **Me-DAPP**$^{2+}$ in MeCN upon excitation at 339 nm, 1.6 μM. (c) Normalized spectra showing the overlap between emission of the **Me-ExBIPY**$^{2+}$ and the absorption of the **Me-DAPP**$^{2+}$. (d) Overlap between the excitation spectrum (λ_{em} = 554 nm) and the UV/vis absorption spectrum of **DAPPBox**$^{4+}$.

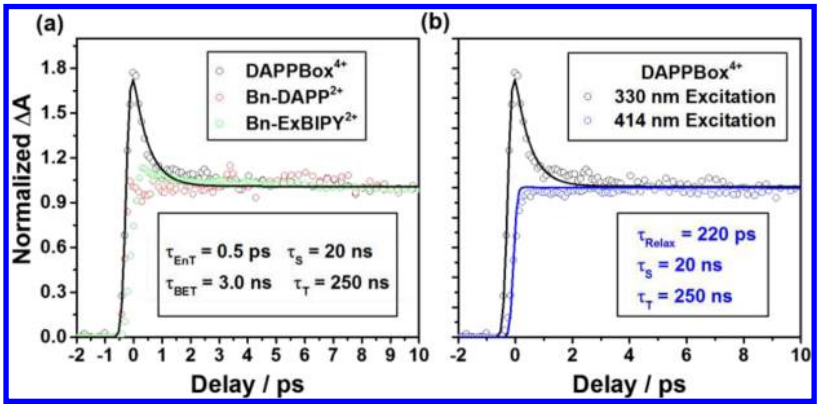

Figure 8. Kinetic decays at 495 nm for (a) **DAPPBox**$^{4+}$ (black), **Bn-DAPP**$^{2+}$ (red), and **Bn-ExBIPY**$^{2+}$ (green) following 60 fs, 330 nm (1 μJ/pulse) excitation and (b) **DAPPBox**$^{4+}$ excited at 330 nm (black) and 414 nm (blue). Only the first 10 ps are shown in order to highlight the ultrafast decay of the **DAPPBox**$^{4+}$ trace, which is not present in the reference compounds. The fit of the full DAPPBox^{4+} kinetic decay is also shown; nanosecond lifetimes obtained from nsTA spectroscopy (Figures S35−S37). All traces were normalized to their respective values at 8 ps.

DAPP^{2+} unit within the cyclophane. Such relative quenching and enhancement were not observed in an equimolar physical mixture of **Me-ExBIPY**$^{2+}$ and **Me-DAPP**$^{2+}$, indicating that efficient EnT processes occur only within the cyclophane. This result can be rationalized by consideration of the conformation of the cyclophane which imparts (i) a reasonable spatial separation (7.1 Å, measured from single crystal structure, Figure 2b) between the energy donor (ExBIPY^{2+}) and acceptor (DAPP^{2+}) in **DAPPBox**$^{4+}$, (ii) a face-to-face chromophore arrangement that aligns the transition dipole moments, and (iii) rigidity that limits conformational flexibility. The high efficiency of EnT is also in line with the favorable overlap (Figure 7c) of the emission spectra of **Me-ExBIPY**$^{2+}$ and the absorption spectra of **Me-DAPP**$^{2+}$, as required for Förster energy transfer. Moreover, the almost perfect matching of the fluorescence excitation spectrum (λ_{em} = 554 nm) and the UV/vis absorption spectrum (Figure 7d) of **DAPPBox**$^{4+}$, once again, corroborates the assignment of EnT process within **DAPPBox**$^{4+}$.

The fsTA spectra support the observation of efficient energy transfer from ^{1}*ExBIPY^{2+} to DAPP^{2+} deduced from the fluorescence data. The fsTA spectra of **DAPPBox**$^{4+}$ following 330 nm excitation show (Figure 6a) increased intensity of the absorption band at 495 nm during the first few picoseconds after excitation compared to those of **Bn-DAPP**$^{2+}$ (Figure S18a), and **DAPPBox**$^{4+}$ following 414 nm excitation (Figure S19a), suggesting the brief appearance of the locally excited state ^{1}*ExBIPY^{2+} (Figure S21a). This relative enhancement does not appear in the spectra of Me-DAPP^{2+} (Figure S15a) or **Bn-DAPP**$^{2+}$ (Figure S18a) nor does it appear in the spectra of **DAPPBox**$^{4+}$ when only the DAPP^{2+} unit is excited (Figures 6b and S19a). Figure 8a shows a comparison of the kinetics at 495 nm for **DAPPBox**$^{4+}$ with **Me-ExBIPY**$^{2+}$ and **Me-DAPP**$^{2+}$ under identical conditions, while Figure 8b shows the kinetic fits for **DAPPBox**$^{4+}$ when the ExBIPY^{2+} and DAPP^{2+} units are excited at 330 and 414 nm, respectively. Scatter of the 505 nm pump prevented the use of that data set for this comparison.

DOI: 10.1021/jacs.6b13223
J. Am. Chem. Soc. 2017, 139, 4107−4116

Upon fitting the kinetic decay at 495 nm, we determined that the energy transfer occurs with a 0.5 ps time constant, which shows that energy transfer from ^{1}*ExBIPY^{2+} to DAPP^{2+} is highly efficient and outcompetes other deactivation pathways previously observed[9] in **ExBox**$^{4+}$.

The rate of resonance EnT can be calculated using Förster theory based on the spectral overlap between the absorption of the **Me-ExBIPY**$^{2+}$ acceptor and the emission of the **Me-DAPP**$^{2+}$ donor. We have calculated the Förster EnT rate with the PhotochemCAD software package,[19] using the steady-state spectra, the fluorescence quantum yield of the donor, the distance between the donor and acceptor from the XRD data,[13] and the refractive index of the MeCN as inputs. The fixed parallel orientation of the donor and acceptor units in **DAPPBox**$^{4+}$ leads to an orientation factor of $\kappa^2 = 1$, as opposed to the typical value of $\kappa^2 = 2/3$ for freely rotating molecules where reorientation occurs faster than the emission time scale. The calculated EnT rate is therefore $k_{EnT} = (0.43\ ps)^{-1}$, a value which is in excellent agreement with the experimental result of $k_{EnT} = (0.5\ ps)^{-1}$ and supports the Förster mechanism. Dexter energy transfer cannot be entirely ruled out, however, since there may be sufficient electronic wave function overlap between the donor and acceptor units to enable ultrafast electron transfer (*vide infra*).

Computational modeling of **^{1}*DAPPBox**$^{4+}$ using time-dependent density functional theory (TDDFT) predicts the first two major absorption peaks at 451 and 352 nm, which correspond to ^{1}*DAPP^{2+} and ^{1}*ExBIPY^{2+}, respectively, in good agreement with experimental observations. The electronic configuration of ^{1}*ExBIPY^{2+} is mainly composed of contributions from molecular orbitals (MOs) of the ExBIPY^{2+} unit, while the 451 nm excitation of the DAPP^{2+} unit involves (Figure S41) contributions from the MOs of the *p*-xylylene linkers and the DAPP^{2+} unit. The total quantum yield from emission of the **DAPPBox**$^{4+}$ can be calculated through the product of (i) the EnT efficiency of **DAPPBox**$^{4+}$ (98%, based on competing rates of the ExBIPY^{2+} excited-state lifetime of 1.56 ns, and the **Bn-ExBIPY**$^{2+}$ charge-transfer time of 60 ps), (ii) the photon absorption efficiency of ExBIPY^{2+} at 330 nm (84%, based on extinction coefficients), and (iii) the fluorescence quantum yield of **Bn-DAPP**$^{2+}$ (0.66, excited at 375 nm). The calculated quantum yield of 0.54 (= 0.98 × 0.84 × 0.66), for the cyclophane is slightly higher than the corresponding measured fluorescence quantum yield of 0.39. The difference between the calculated and experimental results can be explained by the difference between the quantum yields of the units in the cyclophane and those of the ExBIPY^{2+} and DAPP^{2+} reference compounds. Other possible means whereby the quantum yield of the cyclophane is decreased may arise from alternative decay pathways, e.g., an increased rate of internal conversion. We, however, have no direct evidence for any other competitive process.

Ultrafast Electron Transfer within DAPPBox^{4+}. The overlapping DAPP^{2+} unit absorption at 330 nm leads to parallel excited-state populations of ^{1}*ExBIPY^{2+} and ^{1}*DAPP^{2+} within **DAPPBox**$^{4+}$, with the majority of the excitation on the ExBIPY moiety. With the observation of ultrafast energy transfer, we expect no significant yield of charge transfer from the *p*-xylylene linker to ^{1}*ExBIPY^{2+} in the **DAPPBox**$^{4+}$ cyclophane, since this electron transfer occurs with a 60 ps time constant in **Bn-ExBIPY**$^{2+}$ and 240 ps in the ExBox^{4+} cyclophane. We also do not observe any of the characteristic absorption bands[10c] for DAPP$^{+\bullet}$, indicating that **^{1}*ExBIPY**$^{2+}$ does not reduce the DAPP^{2+} moiety within DAPPBox^{4+}. If either of these charge-transfer pathways were significant, the fluorescence quantum yield and lifetime of the cyclophane would be substantially lower.[10c]

Scheme 2. Schematic Representation of the Photodriven Charge Redistribution Yielding the DAPP$^{3+\bullet}$−ExBIPY$^{+\bullet}$ Radical Ion-Pair in DAPPBox^{4+}

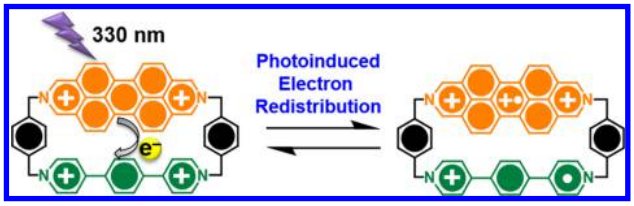

However, the appearance of the 1150 nm band that is similar to the characteristic[14,6c,9] of ExBIPY$^{+\bullet}$ absorption alongside the DAPP suggests that the smaller of these populations decays by ultrafast electron transfer. The red-shift of that band may arise due to Stark effects of the DAPP^{2+} moiety in close proximity. The 1150 nm band appears immediately following excitation and rises over the next few picoseconds. The fit of the **DAPPBox**$^{4+}$ spectra (Figure S37) indicates that the forward electron transfer from 1*DAPP^{2+} to ExBIPY^{2+} occurs in τ_{FET} = 1.5 ps. Therefore, we rule out transfer from the *p*-xylyl linker to ExBIPY (vide supra). Back electron transfer then follows in τ_{BET} = 3.2 ± 0.8 ns. The back-electron-transfer time from the global fits of the fsTA data is consistent with the τ = 2.2 ± 1.2 ns decay observed in the nsTA data (Figure S40). Additionally, as discussed above, no evidence for electron transfer from the *p*-xylyl linker to DAPP^{2+} was observed in the Bn-DAPP^{2+} reference compound, suggesting that the 1150 nm absorption originates from the DAPP$^{3+\bullet}$−ExBIPY$^{+\bullet}$ radical ion pair (Scheme 2).

It should be noted that there is an absorption band present at 1520 nm. However, this band is not an indicator of electron transfer but rather is characteristic of the S_1 state for **Bn-DAPP**$^{2+}$ (Figure S19) as a result of the 505 nm excitation, since (i) this 1520 nm absorption band in the NIR persists for the entire singlet lifetime (~20 ns as confirmed by time-resolved fluorescence) in the case of both **Bn-DAPP**$^{2+}$ (Figure S19) and **DAPPBox**$^{4+}$ (Figure 6b) when excited at 505 nm, and (ii) this band is also similar to the 1430 nm absorption band for **Me-DAPP**$^{2+}$ (no electron transfer possible when excited at 505 nm), shifted, however, by ~50 meV (~400 cm^{-1}). The red shift of the band wavelength can be explained by substituent effects.

The excitation wavelength dependence of the fsTA signal indicates that electron transfer originates from a higher excited state of DAPP^{2+}. The cyclic voltammogram in Figure S7 shows that the oxidation potential of DAPP^{2+} in MeCN is 1.69 V vs Ag/AgCl, while the reduction potential of ExBIPY^{2+} has been reported previously as −0.65 V vs Ag/AgCl.[8a] Using the Weller equation, we can estimate the energy of the DAPP$^{3+\bullet}$−ExBIPY$^{+\bullet}$ radical ion-pair state in MeCN as $\Delta G_{IP} \approx E_{ox} - E_{red}$ = 2.34 eV, and the free energy of photoinduced electron transfer from the various accessible excited states with singlet energy E_S is $\Delta G_{ET} \approx \Delta G_{IP} - E_S$. From this estimate, we see that electron transfer from S_1 of DAPP^{2+} at 2.46 eV is only slightly thermodynamically favorable. However, the solvent reorganization energy is around ~1 eV in this solvent,[6f] and Marcus theory predicts that the ET rate should be relatively slow. It is worth noting that the ion-pair energy obtained from the Weller

DOI: 10.1021/jacs.6b13223
J. Am. Chem. Soc. 2017, 139, 4107−4116

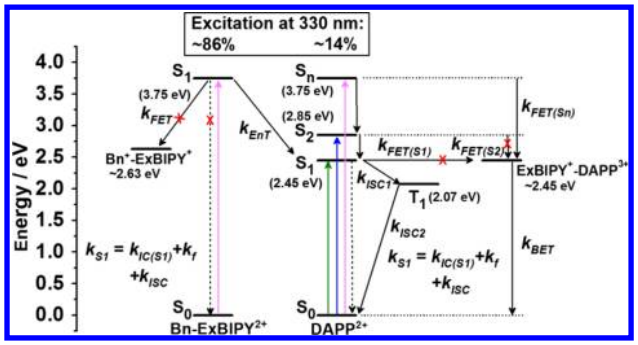

Figure 9. Schematic of the excited-state relaxation pathways in DAPPBox^{4+} at different excitation wavelengths (IC = internal conversion; ISC = intersystem crossing; f = fluorescence; FET = forward electron transfer; BET = back electron transfer; EnT = energy transfer). Dashed arrows indicated radiative transitions. Red X's indicate kinetically unfavorable processes.

equation is likely an overly simplistic approximation. From DFT (see Supporting Information for details), we calculate the lowest energy ion-pair state to be around 2.47 eV; the ∼+0.13 eV difference from the Weller estimate is enough to make ET from the DAPP^{2+} S_1 state thermodynamically unfavorable.

Interestingly, no ET is observed when exciting to the next higher energy excited state at 505 nm ($S_1 \leftarrow S_0$ transition), or even 414 nm (higher vibronic band of the ∼2.85 eV $S_2 \leftarrow S_0$ transition), even though ΔG_{ET} is more negative. It is likely that the rate of internal conversion between the S_2 and S_1 states ($\Delta E_S = -0.40$ eV) is substantially faster than that of ET, effectively shutting off the latter process. Thus, we rule out ET from the lower energy excited states of DAPP^{2+} as a major source of the ion-pair population.

Only when exciting at 330 nm (3.76 eV) do we observe the radical ion-pair absorption, implying that ET is at least competitive with other decay pathways and is perhaps the dominant process from this state. From the energy gap law for nonradiative decay processes, we expect internal conversion from this state (S_n) to the lower lying S_2 state (with gap $\Delta E_S = -0.91$ eV) to be slower than that from S_2 to S_1. At the same time, Marcus theory predicts that with $\Delta G_{ET} \approx -1.41$ eV (−1.38 eV using the DFT ion-pair energy), the ET rate from the vertically prepared S_n state will be much closer to the top of the Marcus rate vs free energy curve, and faster than that for ET from S_2 or S_1. Thus, the combination of faster ET and slower IC processes leads to measurable population of the ion-pair state when exciting at 330 nm; the slower internal conversion from S_n serves as a minor "bottleneck" for relaxation, allowing ET to proceed. The excited-state dynamics of **DAPPBox^{4+}** at each excitation wavelength are summarized in Figure 9.

CONCLUSION

We report the stepwise synthesis of a rationally designed multichromophoric donor−acceptor cyclophane, **DAPPBox^{4+}**. We demonstrate that the use of pyrene as a template favors the formation of this constitutionally asymmetric cyclophane in 35% yield. The structure of **DAPPBox^{4+}** was determined by ^{1}H NMR spectroscopy, high-resolution mass spectrometry in solution, and single-crystal X-ray diffraction analysis in the solid state. Investigations carried out on the photophysical properties of the cyclophane excited at 330 nm by means of steady-state as well as time-resolved absorption and emission spectroscopies reveal not only efficient energy transfer from the ^{1}*ExBIPY^{2+} to the DAPP^{2+} unit in $\tau = 0.5$ ps, but also the existence of an efficient, ultrafast intramolecular electron-transfer pathway: *DAPP^{2+}−ExBIPY^{2+} → DAPP$^{3+\bullet}$−ExBIPY$^{+\bullet}$ radical ion pair in $\tau = 1.5$ ps. The photophysical investigations were also supported by TDDFT results. This class of constitutionally asymmetric cyclophanes may have considerable potential for integration into solar energy conversion and organic electronics. In the context of artificial photosynthesis, the next logical step toward utilizing **DAPPBox^{4+}** will be to bind different guest molecules inside the cyclophane, forming 1:1 complexes, which can serve to modulate the electron-transfer rates.

EXPERIMENTAL SECTION

3. 3,4,9,10-Tetrakis(chloromethyl)perylene[15] (**2**) (623 mg, 4.53 mmol) was added with stirring to a solution of 4-(aminomethyl)benzenemethanol[16] (**1**) (135 mg, 0.302 mmol) in Me_2SO (8 mL) at room temperature. After 5 h, deionized H_2O (100 mL) was added to the reaction mixture, forming a dark yellow precipitate, which was filtered off and then washed with deionized H_2O and a small amount of EtOH, before being dried under vacuum to afford (147 mg, 85%) a dark yellow solid **3**. The product was used without further purification in the next step. ^{1}H NMR (500 MHz, CD_3SOCD_3): δ_H = 8.20 (d, J = 7.7 Hz, 4H), 7.32 (q, J = 8.0 Hz, 8H), 7.24 (d, J = 7.7 Hz, 4H), 4.50 (d, J = 5.7 Hz, 4H), 3.86 (s, 8H), 3.75 (s, 4H). ^{13}C NMR (126 MHz, CD_3SOCD_3): δ_C = 140.8, 135.7, 132.7, 128.1, 125.1, 122.6, 119.1, 62.1, 60.3, 55.2. More detailed discussion of this reaction is available in the Supporting Information.

4·2PF$_6$. DDQ (240 mg, 1.057 mmol) was added to a dark yellow solution of 3 (100 mg, 0.182 mmol) in DMF (8 mL) at room temperature. The color of the reaction mixture became dark brown upon the addition of the DDQ. After stirring for 8 h, a satd aqueous solution (100 mL) of NH_4PF_6 was added to the reaction mixture. The resulting precipitate was filtered off and then washed with deionized H_2O and a small amount of EtOH, before being dried under vacuum to afford (138 mg, 90%) a dark brown solid **4**·2PF$_6$. The crude product was dissolved in MeCN in order to exchange the anions from PF_6^- to Cl^- by addition of an excess of tetrabutylammonium chloride (TBACl). The crude dibromide was then subjected to reverse-phase HPLC, starting with H_2O/0.1% TFA as eluent and adding up to 100% of MeCN/0.1% TFA to the eluent within 40 min. The pure fractions were collected and concentrated under vacuum. The residue was dissolved in H_2O, followed by the addition of NH_4PF_6 to yield pure **4**·2PF$_6$ (124 mg, 80%). ^{1}H NMR (500 MHz, CD_3SOCD_3): δ_H = 10.39 (s, 4H), 9.94 (s, 4H), 8.95 (s, 4H), 7.72 (d, J = 7.9 Hz, 4H), 7.45 (d, J = 7.8 Hz, 4H), 6.41 (s, 4H), 4.53 (s, 4H). ^{13}C NMR (126 MHz, CD_3SOCD_3): δ_C = 150.4, 138.4, 128.3, 128.3, 126.5, 126.2, 113.7, 100.3, 61.8.

BrDAPP·2PF$_6$. **4**·2PF$_6$ (100 mg, 0.116 mmol) was dissolved in MeCN (15 mL), and PBr_3 (100 μL, 1.063 mmol) was added slowly while stirring at room temperature overnight. A saturated aqueous solution (100 mL) of NH_4PF_6 was added to quench the reaction, resulting in the formation of a reddish brown solid. The resulting precipitate was filtered off and then washed with deionized H_2O and a small amount of EtOH, before being dried under vacuum to afford (80 mg, 70%) a reddish brown solid BrDAPP·2PF$_6$. ^{1}H NMR (500 MHz, CD_3SOCD_3): δ_H = 10.44 (s, 4H), 10.04 (d, J = 9.6 Hz, 4H), 9.04 (d, J = 9.3 Hz, 4H), 7.72 (d, J = 7.9 Hz, 4H), 7.60 (d, J = 8.0 Hz, 4H), 6.45 (s, 4H), 4.74 (s, 4H). ^{13}C NMR (126 MHz, CD_3SOCD_3): δ_C = 161.7, 138.8, 129.5, 128.7, 127.7, 127.2, 126.1, 63.7, 39.0, 33.0.

DAPPBox·4PF$_6$. A solution of BrDAPP·2PF$_6$ (1 equiv), ExBIPY (1 equiv), and pyrene (6 equiv) in dry MeCN was stirred at room temperature for 7 days. Excess of TBACl was added to quench the reaction, and the resulting crude precipitate was then dissolved in H_2O. The pyrene template was removed by continuous liquid−liquid extraction with $CHCl_3$ and H_2O over 3 days. The aqueous phase was concentrated to a small volume and then subjected to reverse-phase

DOI: 10.1021/jacs.6b13223
J. Am. Chem. Soc. 2017, 139, 4107−4116

HPLC, starting with H_2O/0.1% TFA as eluent, and adding up to 100% of MeCN/0.1% TFA as eluent within 45 min. The pure fractions were collected and concentrated in vacuum. The residue was dissolved in H_2O, followed by the addition of NH_4PF_6 to afford pure DAPPBox·$4PF_6$ in 35% yield. ^{1}H NMR (500 MHz, CD_3CN): δ_H = 9.96 (s, 4H), 9.65 (s, 4H), 8.86 (s, 4H), 8.65 (d, J = 6.1 Hz, 4H), 7.95−7.83 (m, 8H), 7.61 (d, J = 8.0 Hz, 4H), 7.54 (s, 4H), 6.28 (s, 4H), 5.62 (s, 4H). ^{13}C NMR (126 MHz, CD_3CN): δ_C = 144.5, 138.2, 130.8, 130.6, 129.3, 127.0, 126.0, 66.4, 64.5. HRMS (ESI) for DAPPBox·$4PF_6$; Calcd for $C_{56}H_{40}F_{24}N_4P_4$: m/z = 1203.2174 $[M - PF_6]^+$; Found: 1203.2173 $[M - PF_6]^+$; 529.1266 $[M - 2PF_6]^{2+}$; Found: 529.1263 $[M - 2PF_6]^{2+}$; 304.4293 $[M - 3PF_6]^{3+}$; Found: 304.4293 $[M - 3PF_6]^{3+}$.

Single-Crystal X-ray Diffraction (XRD). *DAPPBox·4TFA. (a) Method.* A 0.25 mM MeCN solution of DAPPBox·4TFA was filtered through a 0.45-μm syringe filter into VWR culture tubes. The culture tubes were placed in one closed 20 mL scintillation vial containing 3 mL iPr$_2$O. After 7 days, reddish brown crystals of DAPPBox·4TFA were obtained. A suitable crystal was selected and mounted in inert oil and transferred to the cold gas stream of a Bruker Kappa APEX CCD area detector diffractometer. The crystal was kept at 100 K during data collection. Using Olex2,[17] the structure was solved with the XM[18] structure solution program using Dual Space and refined with the XL refinement package using least-squares minimization.

(b) Crystal Parameters. DAPPBox·4TFA, orange needles, M = 2442.00, crystal size 0.124 × 0.122 × 0.02 mm^3, triclinic, space group $P\bar{1}$; a = 13.3141(7), b = 21.1146(10), and c = 23.4964(13) Å; α = 96.654(4), β = 99.661(4), and γ = 105.932(4)°; V = 6169.5(6) Å^3, ρ_{calc} = 1.315, T = 100 K, Z = 2; $R_1(F^2 > 2\sigma F^2)$ = 0.0982, wR_2 = 0.2196. Out of 26 407 reflections, a total of 25 028 were unique. Crystallographic data (excluding structure factors) for this structure have been deposited with the Cambridge Crystallographic Data Center as supplementary publication no. CCDC 1480961.

■ ASSOCIATED CONTENT

Supporting Information

The Supporting Information is available free of charge on the ACS Publications website at DOI: 10.1021/jacs.6b13223.

Experimental details, including synthesis, NMR, UV/vis/NIR, fluorescence emission and excitation, fsTA data, and electrochemical experiments (PDF)

X-ray crystallographic data for pyrene⊂**DAPPBox**·$4PF_6$ (CIF)

■ AUTHOR INFORMATION

Corresponding Authors

*m-wasielewski@northwestern.edu

*stoddart@northwestern.edu

ORCID

Ryan M. Young: 0000-0002-5108-0261

Hai Xiao: 0000-0001-9399-1584

Peng Li: 0000-0002-4273-4577

Jiawang Zhou: 0000-0002-2399-0030

Tao Cheng: 0000-0003-4830-177X

William A. Goddard III: 0000-0003-0097-5716

Omar K. Farha: 0000-0002-9904-9845

Joseph T. Hupp: 0000-0003-3982-9812

Michael R. Wasielewski: 0000-0003-2920-5440

J. Fraser Stoddart: 0000-0003-3161-3697

Author Contributions

#X.G. and R.M.Y. contributed equally.

Notes

The authors declare no competing financial interest.

■ ACKNOWLEDGMENTS

This research was conducted as part of the Joint Center of Excellence in Integrated Nanosystems at King Abdulaziz City for Science and Technology (KACST) and Northwestern University (NU). The authors thank both KACST and NU for their continued support of this research. This work was also supported by the Chemical Sciences, Geosciences, and Biosciences Division, Office of Basic Energy Sciences, U.S. Department of Energy (DOE) under grant no. DE-FG02-99ER14999 (M.R.W.). J.T.H. and O.K.F. gratefully acknowledge financial support by the U.S. DOE, Office of Science, Office of Basic Energy Sciences (grant No. DE-FG02 87ER13808) and Northwestern University. H.X. and W.A.G. were supported by NSF (EFRI-00155EI-1332411).

■ REFERENCES

(1) (a) Brédas, J.-L.; Beljonne, D.; Coropceanu, V.; Cornil, J. *Chem. Rev.* **2004**, *104*, 4971. (b) Kirner, S.; Sekita, M.; Guldi, D. M. *Adv. Mater.* **2014**, *26*, 1482.

(2) (a) Vura-Weis, J.; Abdelwahed, S. H.; Shukla, R.; Rathore, R.; Ratner, M. A.; Wasielewski, M. R. *Science* **2010**, *328*, 1547. (b) Goransson, E.; Emanuelsson, R.; Jorner, K.; Markle, T. F.; Hammarstrom, L.; Ottosson, H. *Chem. Sci.* **2013**, *4*, 3522. (c) Strauss, V.; Margraf, J. T.; Dirian, K.; Syrgiannis, Z.; Prato, M.; Wessendorf, C.; Hirsch, A.; Clark, T.; Guldi, D. M. *Angew. Chem., Int. Ed.* **2015**, *54*, 8292.

(3) (a) Aratani, N.; Kim, D.; Osuka, A. *Acc. Chem. Res.* **2009**, *42*, 1922. (b) Patwardhan, S.; Sengupta, S.; Siebbeles, L. D. A.; Würthner, F.; Grozema, F. C. *J. Am. Chem. Soc.* **2012**, *134*, 16147. (c) Parkinson, P.; Knappke, C. E. I.; Kamonsutthipaijit, N.; Sirithip, K.; Matichak, J. D.; Anderson, H. L.; Herz, L. M. *J. Am. Chem. Soc.* **2014**, *136*, 8217. (d) Ragoussi, M.-E.; Katsukis, G.; Roth, A.; Malig, J.; de la Torre, G.; Guldi, D. M.; Torres, T. *J. Am. Chem. Soc.* **2014**, *136*, 4593. (e) Sukegawa, J.; Schubert, C.; Zhu, X.; Tsuji, H.; Guldi, D. M.; Nakamura, E. *Nat. Chem.* **2014**, *6*, 899. (f) Rousseaux, S. A. L.; Gong, J. Q.; Haver, R.; Odell, B.; Claridge, T. D. W.; Herz, L. M.; Anderson, H. L. *J. Am. Chem. Soc.* **2015**, *137*, 12713. (g) Tanaka, T.; Osuka, A. *Chem. Soc. Rev.* **2015**, *44*, 943. (h) Antoniuk-Pablant, A.; Kodis, G.; Moore, A. L.; Moore, T. A.; Gust, D. *J. Phys. Chem. B* **2016**, *120*, 6687.

(4) Galindo, J. F.; Atas, E.; Altan, A.; Kuroda, D. G.; Fernandez-Alberti, S.; Tretiak, S.; Roitberg, A. E.; Kleiman, V. D. *J. Am. Chem. Soc.* **2015**, *137*, 11637.

(5) Ricks, A. B.; Brown, K. E.; Wenninger, M.; Karlen, S. D.; Berlin, Y. A.; Co, D. T.; Wasielewski, M. R. *J. Am. Chem. Soc.* **2012**, *134*, 4581.

(6) (a) Schmidt-Mende, L.; Fechtenkötter, A.; Müllen, K.; Moons, E.; Friend, R. H.; MacKenzie, J. D. *Science* **2001**, *293*, 1119. (b) Gunderson, V. L.; Smeigh, A. L.; Kim, C. H.; Co, D. T.; Wasielewski, M. R. *J. Am. Chem. Soc.* **2012**, *134*, 4363. (c) Young, R. M.; Dyar, S. M.; Barnes, J. C.; Juríček, M.; Stoddart, J. F.; Co, D. T.; Wasielewski, M. R. *J. Phys. Chem. A* **2013**, *117*, 12438. (d) Gallego, M.; Calbo, J.; Aragó, J.; Krick Calderon, R. M.; Liquido, F. H.; Iwamoto, T.; Greene, A. K.; Jackson, E. A.; Pérez, E. M.; Ortí, E.; Guldi, D. M.; Scott, L. T.; Martín, N. *Angew. Chem., Int. Ed.* **2014**, *53*, 2170. (e) Ryan, S. T. J.; Del Barrio, J.; Ghosh, I.; Biedermann, F.; Lazar, A. I.; Lan, Y.; Coulston, R. J.; Nau, W. M.; Scherman, O. A. *J. Am. Chem. Soc.* **2014**, *136*, 9053. (f) Ryan, S. T. J.; Young, R. M.; Henkelis, J. J.; Hafezi, N.; Vermeulen, N. A.; Hennig, A.; Dale, E. J.; Wu, Y.; Krzyaniak, M. D.; Fox, A.; Nau, W. M.; Wasielewski, M. R.; Stoddart, J. F.; Scherman, O. A. *J. Am. Chem. Soc.* **2015**, *137*, 15299.

(7) (a) Lee, C. Y.; Farha, O. K.; Hong, B. J.; Sarjeant, A. A.; Nguyen, S. T.; Hupp, J. T. *J. Am. Chem. Soc.* **2011**, *133*, 15858. (b) Oelsner, C.; Herrero, M. A.; Ehli, C.; Prato, M.; Guldi, D. M. *J. Am. Chem. Soc.* **2011**, *133*, 18696. (c) Jin, S.; Son, H.-J.; Farha, O. K.; Wiederrecht, G. P.; Hupp, J. T. *J. Am. Chem. Soc.* **2013**, *135*, 955. (d) Son, H.-J.; Jin, S.; Patwardhan, S.; Wezenberg, S. J.; Jeong, N. C.; So, M.; Wilmer, C. E.; Sarjeant, A. A.; Schatz, G. C.; Snurr, R. Q.; Farha, O. K.; Wiederrecht, G. P.; Hupp, J. T. *J. Am. Chem. Soc.* **2013**, *135*, 862. (e) Young, R. M.;

DOI: 10.1021/jacs.6b13223
J. Am. Chem. Soc. 2017, 139, 4107−4116

Jensen, S. C.; Edme, K.; Wu, Y.; Krzyaniak, M. D.; Vermeulen, N. A.; Dale, E. J.; Stoddart, J. F.; Weiss, E. A.; Wasielewski, M. R.; Co, D. T. *J. Am. Chem. Soc.* **2016**, *138*, 6163.

(8) (a) Barnes, J. C.; Juríček, M.; Strutt, N. L.; Frasconi, M.; Sampath, S.; Giesener, M. A.; McGrier, P. L.; Bruns, C. J.; Stern, C. L.; Sarjeant, A. A.; Stoddart, J. F. *J. Am. Chem. Soc.* **2013**, *135*, 183. (b) Barnes, J. C.; Juríček, M.; Vermeulen, N. A.; Dale, E. J.; Stoddart, J. F. *J. Org. Chem.* **2013**, *78*, 11962. (c) Dale, E. J.; Vermeulen, N. A.; Juríček, M.; Barnes, J. C.; Young, R. M.; Wasielewski, M. R.; Stoddart, J. F. *Acc. Chem. Res.* **2016**, *49*, 262.

(9) Dyar, S. M.; Barnes, J. C.; Juríček, M.; Stoddart, J. F.; Co, D. T.; Young, R. M.; Wasielewski, M. R. *Angew. Chem., Int. Ed.* **2014**, *53*, 5371.

(10) (a) Slama-Schwok, A.; Jazwinski, J.; Béré, A.; Montenay-Garestier, T.; Rougée, M.; Hélène, C.; Lehn, J.-M. *Biochemistry* **1989**, *28*, 3227. (b) Slama-Schwok, A.; Rougée, M.; Ibanez, V.; Geacintov, N. E.; Montenay-Garestier, T.; Lehn, J.-M.; Hélène, C. *Biochemistry* **1989**, *28*, 3234. (c) Brun, A. M.; Harriman, A. *J. Am. Chem. Soc.* **1991**, *113*, 8153. (d) Basuray, A. N.; Jacquot de Rouville, H.-P.; Hartlieb, K. J.; Kikuchi, T.; Strutt, N. L.; Bruns, C. J.; Ambrogio, M. W.; Avestro, A.-J.; Schneebeli, S. T.; Fahrenbach, A. C.; Stoddart, J. F. *Angew. Chem., Int. Ed.* **2012**, *51*, 11872. (e) Basuray, A. N.; de Rouville, H.-P. J.; Hartlieb, K. J.; Fahrenbach, A. C.; Stoddart, J. F. *Chem. - Asian J.* **2013**, *8*, 524. (f) Hartlieb, K. J.; Basuray, A. N.; Ke, C.; Sarjeant, A. A.; Jacquot de Rouville, H.-P.; Kikuchi, T.; Forgan, R. S.; Kurutz, J. W.; Stoddart, J. F. *Asian J. Org. Chem.* **2013**, *2*, 225. (g) Sampath, S.; Basuray, A. N.; Hartlieb, K. J.; Aytun, T.; Stupp, S. I.; Stoddart, J. F. *Adv. Mater.* **2013**, *25*, 2740. (h) Hartlieb, K. J.; Witus, L. S.; Ferris, D. P.; Basuray, A. N.; Algaradah, M. M.; Sarjeant, A. A.; Stern, C. L.; Nassar, M. S.; Botros, Y. Y.; Stoddart, J. F. *ACS Nano* **2015**, *9*, 1461. (i) Hou, X.; Ke, C.; Bruns, C. J.; McGonigal, P. R.; Pettman, R. B.; Stoddart, J. F. *Nat. Commun.* **2015**, *6*, 6884.

(11) Functionalized PDIs tend to exhibit increased solubilities in organic solvents. Although examples of the incorporation of a PDI unit, modified at its bay position (Figure 1a), into symmetrical cyclophanes have been report by the Würthner group, functionalization at the bay positions might interfere with binding of guests by the cyclophane, while functionalization at the imide positions with alkyl groups may not be appropriate in a robust cyclophane architecture. See: (a) Schlosser, F.; Moos, M.; Lambert, C.; Würthner, F. *Adv. Mater.* **2013**, *25*, 410. (b) Spenst, P.; Würthner, F. *Angew. Chem., Int. Ed.* **2015**, *54*, 10165.

(12) Hunter, C. A.; Sanders, J. K. M. *J. Am. Chem. Soc.* **1990**, *112*, 5525.

(13) In most cases, the geometry of molecules is not necessarily the same in solution as in the solid state because of thermal and environmental disorder. In the case of the **DAPPBox**$^{4+}$, however, this potential mismatching of distances should be much less of an issue as a consequence of the rigidity of the cyclophane, where the range of accessible geometries in solution is quite limited. Therefore, it is not unreasonable to consider the crystal structure as an "equilibrium geometry" about which the solution-state geometry will fluctuate, as a result of both solvent and thermal fluctuations.

(14) Barnes, J. C.; Fahrenbach, A. C.; Dyar, S. M.; Frasconi, M.; Giesener, M. A.; Zhu, Z.; Liu, Z.; Hartlieb, K. J.; Carmieli, R.; Wasielewski, M. R.; Stoddart, J. F. *Proc. Natl. Acad. Sci. U. S. A.* **2012**, *109*, 11546.

(15) Takahashi, M.; Suzuki, Y.; Ichihashi, Y.; Yamashita, M.; Kawai, H. *Tetrahedron Lett.* **2007**, *48*, 357.

(16) Zheng, J.; Li, Y.; Sun, Y.; Yang, Y.; Ding, Y.; Lin, Y.; Yang, W. *ACS Appl. Mater. Interfaces* **2015**, *7*, 7241.

(17) Dolomanov, O. V.; Bourhis, L. J.; Gildea, R. J.; Howard, J. A. K.; Puschmann, H. *J. Appl. Crystallogr.* **2009**, *42*, 339.

(18) Sheldrick, G. *Acta Crystallogr., Sect. C: Struct. Chem.* **2015**, *71*, 3.

(19) Dixon, J. M.; Taniguchi, M.; Lindsey, J. S. *Photochem. Photobiol.* **2005**, *81*, 212.

DOI: 10.1021/jacs.6b13223
J. Am. Chem. Soc. 2017, 139, 4107−4116